Novel Application of Compressed Sensing in Cylindrical Mode Filtering for Far-Field Antenna Measurements

Zhong Chen[1], Stuart Gregson[2,3], Yibo Wang[1]
[1] ETS-Lindgren, Cedar Park, Texas, USA. {zhong.chen, yibo.wang}@ets-lindgren.com
[2] Next Phase Measurements, USA. stuart.gregson@npmeas.com
[3] Queen Mary University of London, London, UK

***Abstract*— Mode filtering has been shown to be very effective in suppressing spurious reflections in antenna measurements. Specifically, it has been well documented that in the quasi-far-field, the two polarizations are decoupled, making it possible to apply standard cylindrical near-field theory on the amplitude and phase data acquired from a single polarization measurement on a great circle cut [1]. The method was further extended to allow data collected from an unequally spaced angular abscissa by formulating the solution as a pseudo-inversion of the Fourier matrix [2]. This formulation, however, can be prone to spectral leakage because of nonorthogonality of the Fourier basis on an irregularly sampled grid, especially when the positions deviate significantly from the regular grid [2]. In this paper, we propose to use Compressed Sensing (CS) to compute the Cylindrical Mode Coefficients (CMCs), which improves the signal to noise ratio, allowing more accurate recovery of the prominent modes. The CS recovery is tenable because with the coordinate translation of the measurement pattern to the rotation center, the Maximum Radial Extent (MRE) of the antenna under test is greatly reduced, making CMCs quite sparse in the mode domain. The novel application of CS presented in this paper further expands the generality of the mode filtering method, which is now applicable to under-sampled data (at below the Nyquist rate) acquired on positions that grossly deviate from the equally-spaced regular grid.**

Index Terms—Cylindrical Mode Filtering, Compressed Sensing, Reflection Suppression, Echo Reduction.

I. INTRODUCTION

In many applications, it is often sufficient to acquire the far-field patterns of an antenna on the two primary great circle cuts, rather than obtaining the complete two-dimensional pattern. Typically, these measurements are conducted in an anechoic chamber at a far-field distance, or in a Compact Antenna Test Range (CATR). To reduce the effects of multipath reflections, it is well documented [1] that by rotating the antenna under test with an intentional positional offset, and subsequently applying a mathematical translation on the pattern data to translate the antenna back to the rotation center, it is possible to filter out the modes associated with the multipath reflections. Under quasi or true far-field conditions, the two orthogonal field components are decoupled. The cylindrical mode coefficients (CMCs) are related to the co-polarized field component by the Fourier Transform. When the measurement is performed on an equally spaced abscissa, the conversion from the spatial domain to the spectrum domain can be efficiently computed via the Fast Fourier Transform (FFT). It is, however, not always convenient or possible to collect data precisely on a regular grid, either because of equipment accuracy or time constraints. In reference 2, one of the authors of this present paper explored the possibility of obtaining the mode coefficients by solving a system of simultaneous equations using a direct, full matrix inversion from the irregularly spaced data. This entails forming the Fourier matrix with unequal spacings, and pseudo inverting the matrix, for example, by using LSQR algorithm [3]. With the CMCs computed, a filtering function can then be applied to retain the modes associated with the physical dimension of the antenna, suppressing the effects of spurious reflections in the environment which appear as additional parasitic sources. In [2], the authors intentionally introduced a large scattering object in a CATR. Here, antenna pattern data was acquired with and without the perturbing scattering object. The results in [2] demonstrated that as long as the acquired pattern data is not excessively unevenly distributed (with angular positions deviating from the ideal by up to *circa* 0.3°), the matrix inversion method could effectively and accurately reveal the underlying antenna pattern.

The highest order cylindrical modes which can be computed are determined by the angular sampling rate. To accurately recover the modes associated with the antenna, the Nyquist sampling requirement states that the data density should, on average, be sufficiently high to accommodate any significant higher order modes, including those from the scatterers. This prevents aliases from contaminating the antenna modes. Furthermore, unevenly sampled data can result in spectrum leakage [4]. This occurs because the Fourier basis loses its orthogonality when the sampling grid is irregular. In this paper, we will provide further illustration of this phenomenon. Therefore, there exists a practical limitation on the degree of "regularity" of the grid. In practical scenarios, this limitation becomes relevant, such as when qualifying an EMC anechoic

chamber using the cylindrical mode filtering method [5]. In such cases, the angular accuracy of the positioning equipment can often be on the order of ±1°.

It is observed that in the mode filtering scheme described above, the antenna modes occupy only the low order modes. The coordinate translation to relocate the transmit antenna to the rotation center effectively reduces the Maximum Radial Extent (MRE), which represents the farthest distance the antenna extends from the rotation center. As a result, the number of significant CMC terms is greatly reduced since, according to cylindrical mode theory, the mode cutoff is determined by the electrical size of the MRE. In other words, the relevant CMCs are sparsely distributed. This opens up the possibility of treating the problem as a Compressed Sensing (CS) recovery problem. Recent advancements in CS algorithms [6, 7] have made it feasible to effectively solve such problems. Compressed Sensing (CS) can leverage the sparsity of data in the Fourier basis by aiming for a parsimonious solution that contains the fewest non-zero CMCs. By formulating the problem as a CS problem, we not only reduce the number of required sampling points (which can be far fewer than what is prescribed by the Nyquist criterion), but also and crucially, we eliminate the need for data to be collected on an evenly spaced abscissa. In fact, random or pseudo-random sampling becomes a prerequisite and is a distinctive characteristic of the CS approach. In this paper, we will employ the same QMUL CATR measurement dataset as was used in [1, 2], but here with an even greater level of randomness and down-sampling. Our aim here is to demonstrate that the CS algorithm can effectively reconstruct the antenna patterns, even with significantly relaxed sampling requirements. This involves utilizing a substantially smaller number of samples and data points that deviate considerably from the ideal positions. The novel utilization of the CS algorithm in mode filtering applications introduced here significantly broadens its applicability, enabling sub-Nyquist sampling and considerably reducing the requirements for positioning equipment accuracy, although requirements for precision remain.

II. Formulation of the CS Solution

To facilitate the separation of antenna modes from multipath effects, the Antenna Under Test (AUT) is intentionally positioned off-center from the rotation axis. The initial postprocessing step is to reference the antenna pattern back to the rotation center. In the far-field, this is achieved by a phase adjustment:

$$\underline{E_t}(r \to \infty, \phi) = \underline{E}(r \to \infty, \phi) e^{j k_0 \cdot \underline{r}_m} \tag{1}$$

where $\underline{E_t}(r \to \infty, \phi)$ is the translated electric field vector; $\underline{E}(r \to \infty, \phi)$ is the electric field before translation; $\underline{r}_m$ denotes the displacement vector between the center of the measurement coordinate system and the center of the current AUT; k_0 is the free-space wave number. The coordinate system is defined per the usual spherical/cylindrical coordinate convention (where the rotation axis is $\hat{z}$, and the propagation direction is along $\hat{x}$. The center of rotation is at the origin).

The primary factor that leads to the sparsity of CMCs in the mode domain is the coordinate translation accomplished by (1). This translation significantly reduces the effective MRE, thereby concentrating the antenna modes primarily in the lower orders.

The next step is to transform the spatial domain data to the spectrum domain, represented by the sum of CMCs multiplied by their Fourier basis functions. The relationship is given by [1, 2],

$$E_\phi = -2 \sum_{n=-\infty}^{\infty} j^n B_n^1 \mathrm{e}^{\mathrm{j}n\phi} \tag{2a}$$

$$E_\theta = -2j \sum_{n=-\infty}^{\infty} j^n B_n^2 \mathrm{e}^{\mathrm{j}n\phi} \tag{2b}$$

where $B_n^{1,2}$ are the complex CMCs for the TE and TM polarizations, respectively; $E_{\theta,\phi}$ are the electric field representing data acquired for vertical or horizontal polarizations, respectively. When the values $E_{\theta,\phi}$ are obtained on a regular grid, we can solve (2a) and (2b) using the FFT. However, if the values are not acquired on a regular grid, we need to express the equations in the form $Ax = b$. As an example, (2b) for the vertically polarized antennas becomes,

$$-2j \begin{bmatrix} e^{j\frac{2\pi\phi_1}{T}\gamma_1} & e^{j\frac{2\pi\phi_1}{T}\gamma_2} & \cdots & e^{j\frac{2\pi\phi_1}{T}\gamma_N} \\ e^{j\frac{2\pi\phi_2}{T}\gamma_1} & \ddots & & \vdots \\ \vdots & & & \vdots \\ e^{j\frac{2\pi\phi_M}{T}\gamma_1} & e^{j\frac{2\pi\phi_M}{T}\gamma_2} & \cdots & e^{j\frac{2\pi\phi_M}{T}\gamma_N} \end{bmatrix} \begin{bmatrix} j^{\gamma_1} B_{\gamma_1}^2 \\ j^{\gamma_{1+1}} B_{\gamma_{1+1}}^2 \\ \vdots \\ j^{\gamma_K} B_{\gamma_N}^2 \end{bmatrix} = \begin{bmatrix} E_{\theta_1} \\ E_{\theta_2} \\ \vdots \\ E_{\theta_M} \end{bmatrix} \tag{3}$$

Here, T is the range of angular rotation. For example, $T = 2\pi$ for a full rotation; φ_m is the turntable rotation angle at the m^{th} position ($m = 1 \ldots M$); γ_n is the mode index ($n = 1 \ldots N$). The electric field vector on the right-hand side $[E_{\theta_1} \ldots E_{\theta_M}]^T$ is known from the far-field measurement. We seek to invert (3) to solve for the N unknown mode coefficients $[j^{\gamma_1} B_{\gamma_1}^2 \ldots j^{\gamma_K} B_{\gamma_N}^2]^T$. The formulation presented in (3) provides increased flexibility compared to the conventional FFT based approach. First, there are M measurements (or angular data points) and N unknowns (*i.e.* CMCs). Unlike for the case of the FFT, M and N do not need to be equal. Secondly, the angular step size can vary, *i.e.*, allowing irregular step sizes. In the case of $M > N$, we have an overdetermined system of equations. This is the case treated in [2], where (3) is solved in a least squares sense by matrix pseudo inversion. When $M < N$, we have an underdetermined system of equations, for which infinite number of solutions can exist. Within the CS scheme, an additional constraint is imposed to ensure the uniqueness of the solution. Specifically, we aim to obtain a sparse solution that has the minimum number of non-zero mode coefficients (CMCs). That is,

$$\min\{ \|x\|_0 : Ax = b \} \tag{4}$$

where the quantity $\|x\|_0$ denotes the number of non-zero terms in the vector x (known as l_0-norm). Eq. (4) is known to be computationally intractable (combinatorically complex). One approach is to solve for a more relaxed surrogate l_1 optimization, *i.e.*,

$$\min\{\|x\|_1 : Ax = b\} \quad (5)$$

where $\|x\|_1$ is the l_1-norm of the vector x. A comprehensive discussion of the CS principle is beyond the scope of this paper. Interested readers can find more information in the open literature, *e.g.* [6, 7]. To efficiently solve (5), various software packages exist, *e.g.* CVX [8], YALL1 [9], and SPGL1 [10] which are readily accessible and can be employed. For this study, we have chosen to utilize the YALL1 algorithm due to its perceived balance of efficiency and accuracy [11]. Additionally, we incorporated reweighted l_1 minimization [12, 13] to further enhance the recovery performance.

III. Application to Measurement Data

The measurement data utilized in this study corresponds to the dataset presented in [1, 2], which was collected at the Queen Mary University of London (QMUL) mm-wave CATR. The vector pattern data was collected on an X-band corrugated horn antenna. The antenna was offset from the rotation center by approximately 0.145 m. The single offset mm-wave CATR reflector has a diameter of 3 meters. The experimental setup is depicted in Fig. 1, and for more detailed information, please refer to [1, 2]. In Fig. 1, a flat metallic scatterer measuring 0.6 m x 0.6 m was introduced in a specular region to perturb the antenna pattern deliberately and can be seen to the right hand side. This deliberate perturbation served as a severe case of contamination to test the robustness of the mode filtering algorithm. The raw dataset comprises over 3,800 measurement points, acquired on a regular time basis, and was approximately evenly spaced in an angular domain, covering an azimuthal range from -100° to 100°. This oversampling greatly exceeds the Nyquist criteria, allowing for easy down-sampling for the various scenarios needed in this investigation.

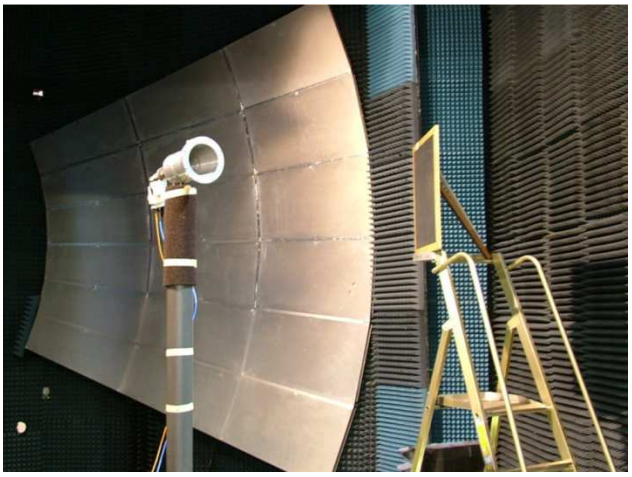

Fig. 1. X-band corrugated horn AUT installed within QMUL CATR shown together with 0.6 m X 0.6 m reflecting plate.

Random and incoherent sampling [6,7] is preferred per the CS theory. In (3), the [A] matrix denotes the Fourier ensemble (Discrete Fourier Transform, or DFT vectors). Randomly selecting rows from the DFT matrix guarantees that we have a linearly independent system of equations and hence promotes a unique solution. It is also known that the DFT basis is not orthogonal on an irregular grid. Therefore, it is suspected that "too much" randomness may also be detrimental, which can introduce excessive spectrum leakage noise, not to mention the potential avoidance of potential specific physical features. Here, we use two different sampling schemes to investigate this effect.

A. Jittered Sampling

In the first case, we down-sample the dataset to M = 121 points using a "pseudo random" scheme. In this scheme, we divide the 200° azimuthal range (of over 3,800 data points) evenly into 121 "bins". In each bin, we randomly select a sample. This is also referred to as "smart" or "jittered" sampling [14-17].

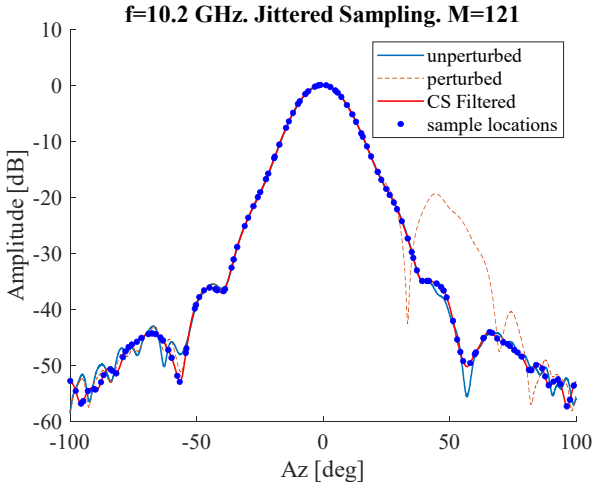

Fig. 2. Far-field amplitude plot of horn measured unperturbed and perturbed, compared against Compressing Sensing using jittered sampling.

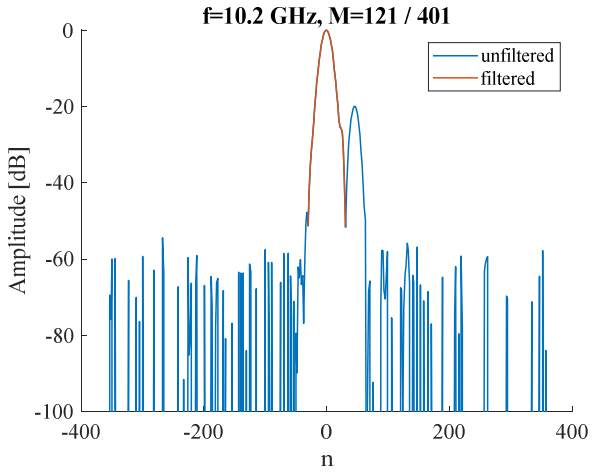

Fig. 3. Plot of amplitude of CMCs as obtained from Compressed Sensing using jittered sampling.

Data selected under this scheme has a constrained randomness in that they satisfy the incoherency requirements of the CS, but unlike completely random sampling are not prone to leaving large gaps between adjacent sample points. In the CS solution, we set N = 401, this represents the number of unknow CMCs. This number should be chosen large enough to include any significant higher order modes which may exist in the raw data. Fig. 2 shows the antenna pattern results using the

CS algorithm. Fig. 3 shows the amplitude of the CMCs as obtained from the CS using the jittered sampling scheme.

The actual sample positions are projected onto the CS curve (as the blue dots in Figs. 2 and 4) to help visualize how the data are sampled. The maximum angular spacing between adjacent data points is 2.9°, which is larger than the sample spacing suggested by the classical sampling theorem.

B. Uncontrained Random Sampling

In the second sampling scheme, we once again sample M = 121 points, but this time they are randomly selected from the raw dataset without any additional constraints. The angular spacings between any adjacent points vary from 0.051° to 8.236°, the latter being many times the sample spacing suggested by the classical sampling theorem. Fig. 4 illustrates the amplitude of the antenna pattern, while Fig. 5 displays the corresponding reconstructed CMCs. Despite a slightly higher error compared to the jittered sampling scheme, the CS algorithm still manages to reasonably recover the antenna pattern. However, the direct matrix inversion using LSQR fails completely when using these randomly selected data. The corresponding spectrum reveals that the noise floor is too high for the matrix inversion method, with only a 20 dB difference from the main peak and only a few low order modes being reproduced reliably.

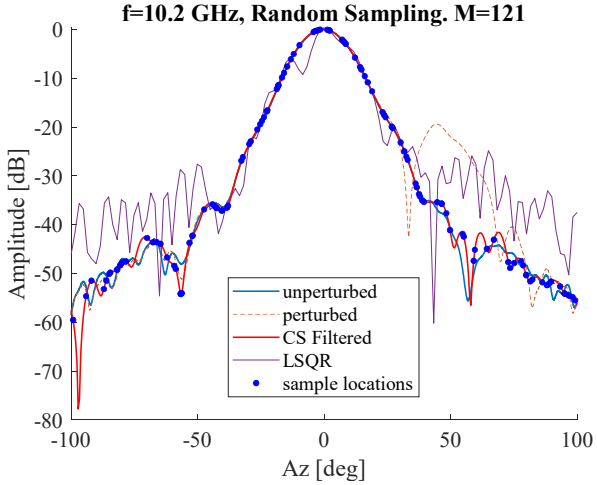

Fig. 4. Far-field amplitude plot of horn measured unperturbed and perturbed, and compared against Compressing Sensing using true random sampling.

It is well understood that under-sampling on a regular grid leads to aliasing, which interferes with the desired modes in a coherent manner. On the other hand, random under-sampling tends to spread the aliased signals over a broader spectrum, resulting in wideband noise-like artifacts. In the context of Compressed Sensing, spread-out "noise" actually creates a favorable condition for recovery. According to the CS theory [7], the accurate recovery of [x] relies on two conditions:

(1) [x] being sufficiently sparse, and

(2) the under-sampling artifacts being incoherent.

Here, it can be shown that broadband spectral artifacts have a diminished influence on the CS recovery process. This can be attributed to the nonlinear nature of the reconstruction, which prioritizes both sparsity and data consistency, consequently confining the detrimental effects of broadband spectral artifacts to only the non-zero spectral components. The same cannot be said for the full matrix inversion method using LSQR. As the least squares solution is typically full ranked, the entire leakage contributes to the matrix inversion, *i.e.*, the solution of the system of equations.

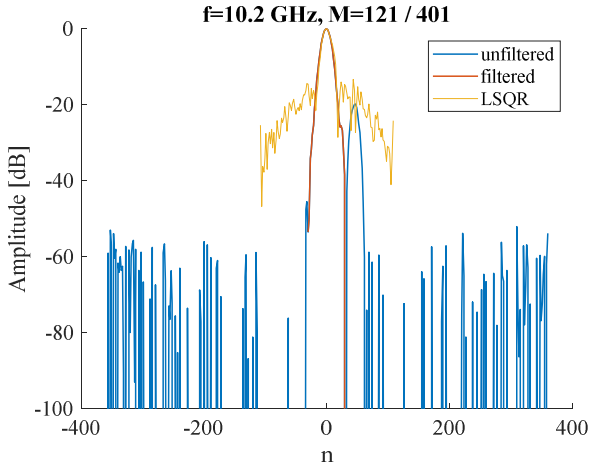

Fig. 5. Plot of amplitude of CMCs as obtained from Compressed Sensing using true random sampling.

The effect of spectral leakage can be illustrated by examining the convolution matrix. Following [14,15,18], we define the convolution matrix as $\mathbf{C} \triangleq \mathbf{A}^H\mathbf{A}$ where $\mathbf{A}$ is the Fourier matrix in (3); $\mathbf{A}^H$ is its Hermitian transpose. For the FFT matrix where data is evenly sampled and above the Nyquist rate, the convolution matrix $\mathbf{A}^H\mathbf{A}$ is fully diagonal, signifying no spectrum leakage. Otherwise, a non-zero off-diagonal element at position (i, j) indicates that the linear reconstruction of element i is affected by interference from a unit impulse at element $j \neq i$. In essence, the presence of non-zero off-diagonal elements in the convolution matrix provides an indication of the extent to which energy disperses from the genuine underlying source element to other elements. For under-sampled and evenly spaced signals, there are structured off-diagonal elements (*cf.* Fig. 6(a)). These off-diagonal elements create aliases. For jittered and random under-sampling, the non-zero off-diagonal elements are much lower in magnitude and spread out to almost the entire matrix (Fig 6(b) and (c)). The second row of Fig. 6 ((d), (e) and (f)) shows the log magnitude of the middle row of the convolution matrix (*i.e.*, representing a view of the convolution kernel). An interesting observation is that in the vicinity of the spectrum's center, the noise level for the jittered sampling approach is lower compared to random sampling (see Fig. 6(e) in contrast to Fig. 6(f)). This lower noise level results in an improved signal-to-noise ratio for the lower-order CMCs, which is precisely where the antenna modes reside and is the region within the mode domain that is of greatest significance. This finding further supports the advantage of the jittered "smart" sampling approach over the truly random sampling scheme.

Moreover, the random sampling scheme has the potential to introduce very large gaps between data points. When such large gaps occur, local effects that display a weak dependency on data from other regions may be overlooked. Conversely, the jittered "smart" sampling approach ensures more comprehensive coverage and reduces the likelihood of missing such local effects.

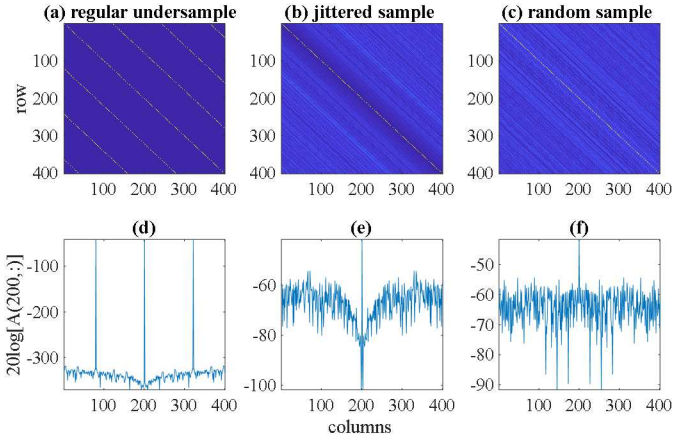

Fig. 6. Convolution matrix (amplitude) for (a) evenly spaced under-sampling (b) jittered sampling (c) random sampling. (d), (e), and (f) shows the mid row cut showing the level of spectral leakage.

IV. Summary and Conclusion

In this research, we present the application of Compressed Sensing to cylindrical mode filtering for the first time. Our primary objective is to effectively suppress spurious reflections in one-dimensional far-field antenna pattern measurements while significantly relaxing the sampling requirements. We demonstrate that even with sub-Nyquist sampling and data collected on a highly irregular grid, accurate antenna patterns can be recovered through post-processing techniques. This significantly broadens the applicability of the mode filtering approach, as it allows for reduced data acquisition time and relaxed positional equipment accuracy.

Furthermore, we investigate two sampling schemes for the Compressed Sensing algorithm. Our findings reveal that the smart jittered approach where the gap size between adjacent data points is controlled yields improved mode recovery compared to purely random sampling.

Acknowledgement

The authors gratefully acknowledge and extend their thanks to Mr. J. Dupuy with Queen Mary University of London (retired) who undertook the experimental portion of this work.

References

[1] S. F. Gregson, J. Dupuy, C. G. Parini, A. C. Newell and G. E. Hindman, "Application of Mathematical Absorber Reflection Suppression to Far-field Antenna Measurements," *2011 Loughborough Antennas & Propagation Conference*, Loughborough, UK, 2011.

[2] S. F. Gregson, C. G. Parini and A. C. Newell, "A General and Effective Mode Filtering Method for the Suppression of Clutter in Far-Field Antenna Measurements," 2018 AMTA Proceedings, Williamsburg, VA, USA, 2018.

[3] C. C. Paige and M. A. Saunders, LSQR: An algorithm for sparse linear equations and sparse least squares, TOMS 8(1), 43-71 (1982).

[4] Sheng Xu, Yu Zhang, Don Pham, and Gilles Lambaré, "Antileakage Fourier Transform for Seismic Data Regularization," GEOPHYSICS 70: V87-V95, 2005.

[5] Z. Chen and Y. Wang, "Generalized Cylindrical Mode Filtered Site VSWR for Above 18 GHz EMC Site Evaluation Using Compressed Sensing," EMC Europe 2023, Krakow.

[6] Candes, E. J., Romberg, J. K. & Tao, T., "Stable Signal Recovery from Incomplete and Inaccurate Measurements", Communications on Pure and Applied Mathematics 59, 1207–1223 (2006).

[7] Donoho, D. L. "Compressed Sensing", *IEEE Trans. Inform. Theory* **52,** 1289–1306 (2006).

[8] Michael Grant and Stephen Boyd, "CVX: Matlab Software for Disciplined Convex Programming, Version 2.0 beta," http://cvxr.com/cvx, September 2013.

[9] YALL1 basic solver code: Y. Zhang, J. Yang, and W. Yin. YALL1: Your ALgorithms for L1, online at yall1.blogs.rice.edu, 2011.

[10] E. van den Berg and M. P. Friedlander, "SPGL1: A Solver for Large-scale Sparse Reconstruction", https://friedlander.io/spgl1/, December 2019.

[11] M. Zambrano, F. Arias and C. Medina, "Comparative Analysis of Sparse Signal Reconstruction Algorithms for Compressed Sensing," Twelth LACCEI Latin American and Caribbean Conference for Engineering and Technology (LACCEI'2014), Ecuador, 2014.

[12] Candes, E. J., Wakin B. W. and Boyd S., "Enhancing Sparsity by Reweighted l_1 Minimization," Journal of Fourier Analysis and Applications (2008) 14: 877-905.

[13] M. S. Asif and J. Romberg, "Fast and Accurate Algorithms for Re-Weighted l_1-Norm Minimization," in *IEEE Transactions on Signal Processing*, vol. 61, no. 23, pp. 5905-5916, Dec. 1, 2013.

[14] Gilles Hennenfent and Felix Herrmann, "Simply Denoise: Wavefield Reconstruction via Jittered Undersampling," Geophysics, Vol. 73, No. 3, May-June, 2008.

[15] Gilles Hennenfent, "Sampling and Recontruction of Seismic Wavefields in the Curvelet Domain", Doctoral Thesis, the University of British Columbia, 2008.

[16] V. M. Patel, G. R. Easley, D. M. Healy and R. Chellappa, "Compressed Sensing for Synthetic Aperture Radar imaging," 2009 16th IEEE International Conference on Image Processing (ICIP), Cairo, Egypt, 2009.

[17] S. F. Gregson, Z. Qin and C. G. Parini, "Compressive Sensing in Massive MIMO Array Testing: A Practical Guide," in IEEE Transactions on Antennas and Propagation, vol. 70, no. 9, pp. 7978-7988, Sept. 2022.

[18] M. Lustig, D. L. Donoho, J. M. Santos and J. M. Pauly, "Compressed Sensing MRI," in IEEE Signal Processing Magazine, vol. 25, no. 2, pp. 72-82, March 2008.